
Spectrally Decomposed Diffusion Models for Generative Turbulence Recovery

Mohammed Sardar
School of Engineering
The University of Manchester
mohammed.sardar@manchester.ac.uk

Alex Skillen
School of Engineering
The University of Manchester

Małgorzata J. Zimon^{1,2}
¹IBM Research Europe
²School of Mathematics,
The University of Manchester

Samuel Draycott
School of Engineering
The University of Manchester

Alistair Revell
School of Engineering
The University of Manchester

Abstract

We investigate the statistical recovery of missing physics and turbulent phenomena in fluid flows using generative machine learning. Here we develop a two-stage super-resolution method using spectral filtering to restore the high-wavenumber components of a Kolmogorov flow. We include a rigorous examination of generated samples through the lens of statistical turbulence. By extending the prior methods to a combined super-resolution and conditional high-wavenumber generation, we demonstrate turbulence recovery on a $8\times$ upsampling task, effectively doubling the range of recovered wavenumbers.

1 Introduction

Numerical approaches to fluid dynamics typically require a compromise between computational accuracy and tractability. The range of length scales in turbulence means that lower-fidelity approaches necessarily lose some characteristics of a flow, while directly solving the governing equations remains computationally infeasible in most cases. Developments in machine learning to increase image resolution and recover missing details present us with generative super-resolution methods, which may be used to recover small-scale turbulent structures from fields produced by lower-fidelity methods. However, despite efforts to capture all scales through super-resolution (SR), small length-scale turbulent structures remain elusive.

Turbulence super-resolution considers the recovery of turbulent structures from lower-resolution fields. Often in low-resolution fields, the sub-grid scale stresses act to alter the resolved field, obscuring high-frequency turbulence information and changing the trajectory of turbulence evolution. As a result, the solution field is not simply a low-pass filtered version of the high-fidelity field. This can make it difficult to infer useful information regarding the impact of turbulence on the resolved fields.

Fukami et al. [1] established that non-generative convolutional methods can be used to super-resolve turbulent flow fields, by exploiting the ability of Convolutional Neural Networks (CNNs) to learn spatial correlations. Their analysis of vorticity distributions and spectra in the reconstructed flows showed that there are limitations to this approach, with many super-resolved samples deviating substantially from the reference Direct Numerical Simulation (DNS). This may be attributed to the fact that CNNs in SR produce blurred images without sharp detail. Attempts to address this were made by Liu et al. [2], by including a temporal component of the data in their super-resolution method. Taking contiguous-in-time snapshots of turbulence as training samples allows for a CNN to

include learnt temporal correlations, and they found that this greatly improved the physical accuracy of their predictions, and reduced blurriness. Limitations of this work include poor performance in viscosity-dominated regions.

The seminal work in super-resolution of turbulence using generative methods by Kim et al. [3] showed that deep learning approaches can be powerful Super-Resolution (SR) tools for turbulence. They highlighted the success of generative methods in super-resolving data from LES data, rather than downsampling high-fidelity data, using a form of Generative Adversarial Network (GAN). It was mathematically shown by Drygala et al. [4] that GANs are able to learn ergodic systems. Ergodic systems are those wherein a single time-evolution of the system will eventually traverse all possible states. The ergodicity hypothesis for turbulence is used frequently as justification for the equivalency between long-in-time time averaging and ensemble averaging approaches [5]. Drygala et al. [4] demonstrated a novel use of segmentation masks with a conditional GAN to synthesise LES samples of flow around a stator blade. This kind of conditioning information is useful in the context of Computational Fluid Dynamics (CFD) because it may be exploited to reproduce numerical boundary conditions and more accurately reproduce flows.

Diffusion models are a novel form of generative method, exploiting useful properties of diffusion processes to generate samples of data [6]. They utilise learnt neural denoising functions to parameterise stochastic processes going from Gaussian noise to new samples of data. Diffusion models have the potential to provide superior quality generation, relative to GANs, while also avoiding several of the key challenges in training GANs such as unstable training modes and mode collapse [7]. Diffusion models have demonstrated superior performance compared to GANs for image synthesis [8], albeit with an increased inference cost.

Inspired by recent developments in diffusion models using conditioning information for generation, Shu et al. [9] developed a physics-informed diffusion model for SR of turbulence. They demonstrated that incorporating physics residuals in the conditioning information given to the diffusion model during training can enhance the quality of generated samples as compared to a baseline SR Denoising Diffusion Probabilistic Model (DDPM) [6]. Advances in DDPM-based SR promise that this work can be extended to reduce inference cost and increase generative accuracy [10].

This work aims to improve the statistical recovery of a turbulent flow field, relative to the state of the art in the literature. Several derived quantities including the vorticity field, vorticity Probability Density Function (PDF), and the Turbulent Kinetic Energy (TKE) spectra are computed. These quantities provide a statistical description of the flow field. The spectral information is then used to define a cut-off for our second stage, high-wavenumber turbulence recovery. Initial turbulence recovery is accomplished by a spatial SR model [10], with a secondary recovery of the high-wavenumber structures, using the generated super-resolved low-wavenumber structures as conditioning information. We anticipate that this two-stage approach would allow for turbulence recovery to arbitrary wavenumbers, rather than being confined to perceptual accuracy. We test this method on a Kolmogorov flow [11], at an SR factor of $8\times$, demonstrating statistical recovery of turbulence.

2 Methodology

Here we detail our approach to turbulence recovery on a statistically stationary Kolmogorov flow. By integrating generative machine learning methods with a novel approach to deriving conditioning information from turbulent flow data, we aim to produce a two-stage generative model capable of generating statistically accurate snapshots of turbulence.

2.1 Kolmogorov Flow Data

Training and validation data are obtained from different snapshots of the same statistically stationary flow. The governing equations are the incompressible Navier-Stokes equations in 2D:

$$\begin{aligned} \frac{\partial u_i}{\partial t} + u_j \frac{\partial u_i}{\partial x_j} &= -\frac{\partial p}{\partial x_i} + \nu \frac{\partial^2 u_i}{\partial x_j \partial x_j} + f_i, \\ \frac{\partial u_i}{\partial x_i} &= 0, \end{aligned} \tag{1}$$

where u_i is the velocity field, x_i is the distance measure, p is the pressure, ν is the kinematic viscosity, $f_i = \sin(10\delta_{i2}x_2)$ is a steady sinusoidal forcing term, and δ is the Dirac delta function. The domain is taken as a square of length 2π in physical space, which for 256×256 grid points leads to a square of 128×128 in wavenumber space. The boundaries are fully periodic. We employ $\nu = 0.0045 \text{ m}^2 \text{ s}^{-1}$ in our simulations, allowing for turbulent dynamics. The equations are solved numerically in the Fourier domain, using a spectral code [12]. The velocity fields are initialised uniformly based on a prescribed peak wavenumber, and are then filtered using white noise generated from a random seed to match a defined spectral density. Data from the initial stages of turbulence evolution is discarded so that the dataset contains only snapshots from the statistically stationary portion of the flow; this range is determined by computing the variation in time of the mean and variance of the velocity.

To ensure statistical independence of samples used during training and validation, the autocorrelation function was used to define the decorrelation period. Using this write frequency, we generated 5000 samples of decorrelated training data. We reset the random seed for flow initialisation and then generated a further 600 samples of decorrelated validation data (also separated by the decorrelation period).

2.2 Diffusion Model

A diffusion model relies on learning the reverse process induced by a Markov chain of Gaussian transitions which act to iteratively add noise to data, transforming a distribution of data to a Gaussian. By learning the reverse process, a diffusion model is able to generate samples of data from pure noise. The forward noising schedule, β , is the variance of the Gaussian transition kernel at each step in the forward process. We define $\alpha = 1 - \beta$, and γ as the cumulative product of α . This can be used to ‘jump’ forwards to a given noising step from $s = 0$, and in effect represents the information degradation in the noising process, starting at 1 and reaching a maximum at $s = S$. Figure 1 presents two noising schedules, one where large-scale information is destroyed quickly, and another where this information is destroyed more gradually. The choice of noising schedule is a hyperparameter; Chen [13] presents an in-depth discussion on noise scheduling strategies, their impact on training, and on generation quality.

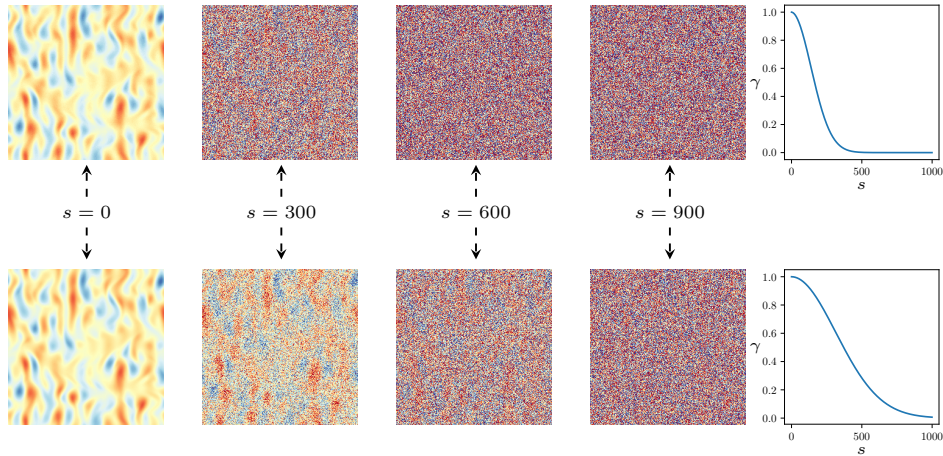


Figure 1: A comparison of two noising schedules in terms of their impact on a sample from the dataset, with the last column showing the two γ schedules. Top (linear): $\beta_0 = 1\text{e-}4$, $\beta_S = 5\text{e-}2$. Bottom (linear): $\beta_0 = 1\text{e-}5$, $\beta_S = 1\text{e-}2$. The 0 subscript denotes initial value, and S is the final step in the variance schedule.

We use a DDPM [6] with the SR3 formulation [10] to super-resolve an average pooled velocity field. A UNet [14] CNN is used as the backbone of our diffusion model. During training, we show the diffusion model Low-Resolution (LR) average-pooled DNS samples, and corresponding High-Resolution DNS (HR) samples from a given instance of DNS for spatial super-resolution. High-resolution samples are put through the forward noising process (Figure 1), and concatenated to their counterpart low-resolution samples. This is fed through the UNet, which is trained to predict the noise added to the HR sample while also suitably conditioning on the low resolution information available. In effect, the UNet is trained to be a denoising function.

Daras et al. [15] and Lai et al. [16] demonstrate that enforcing properties of underlying stochastic processes can improve generative performance of diffusion models. We observed that fine-tuning a trained model on a consistency objective [15] drove the UNet towards an idealised denoising function, and that relaxing some of the imposed constraints did not adversely affect training or generation.

At inference time, the UNet is used as one component of an iterative scheme for generation. Generation is carried out by taking a reverse noising schedule, which takes samples of noise and iteratively traverses the associated reverse Markov chain to generate a new sample from the original data distribution, conditional on the low-resolution sample (i.e. super-resolution). Equation 2 details the iterative scheme used during inference:

$$\mathbf{y}_{s-1} \leftarrow \frac{1}{\sqrt{\alpha_s}} \left(\mathbf{y}_s - \frac{1 - \alpha_s}{\sqrt{1 - \gamma_s}} f_\theta(\mathbf{x}, \mathbf{y}_s, \gamma_s) \right) + \sqrt{1 - \alpha_s} \epsilon_s, \quad (2)$$

where ϵ_s is an instantaneous sample of Gaussian noise, $f_\theta(\mathbf{x}, \mathbf{y}_s, \gamma_s)$ is the UNet prediction of ϵ_s (given the symbol $\hat{\epsilon}$), s is used to denote denoising step, α is defined as before, and \mathbf{y}_s is a sample of pure Gaussian noise being iteratively transformed into a sample of data over S steps, starting from \mathbf{y}_S and going to \mathbf{y}_0 . While \mathbf{x} is used here for low-resolution, in general, it is a tensor of conditioning information. We exploit this fact in our proposed second stage generation, to be discussed. We note that SR3 removes the requirement that the number of steps, S , must be the same for training and inference.

Saharia et al. [10] mentions the possibility of altering their original regression target, ϵ , to the denoised sample, \hat{y}_0 . In our experience, this regression target presented a practical issue: given a low-resolution image, and a noisy high-resolution image, if the training objective is to predict the original sample of data, the UNet will take the ‘easier’ optimisation trajectory and ignore the noisy high-resolution sample, degenerating to a pure super-resolution CNN. What remains to be explored is the use of the \hat{y}_0 regression target in unconditional generation, where a low-resolution sample is not present. In this work, we use the ϵ regression target.

2.3 Fourier Filtering

Fourier transforms allow for analysis of turbulence in wavenumber space. We consider only discrete Fourier transforms, computed using Fast Fourier Transforms (FFT). The maximum wavenumber is the Nyquist wavenumber, defined as $k_{max} = \pi/LN$ for N uniformly spaced grid points along a given axis [17]. Here, as $L = 2\pi$, $k_{max} = 1/2N$. The discrete 2D FFT is given in Eq. 3, and the wavenumber is the magnitude of the wavevector (Eq. 4):

$$\mathcal{F}(\mathcal{F}(u_{x,y})_x)_y = \sum_{m=0}^{N_y-1} \sum_{j=0}^{N_x-1} u_{x,y} e^{-2\pi i(j/N_x + m/N_y)} \quad (3)$$

$$k = |\boldsymbol{\kappa}| = \begin{cases} \left| \begin{matrix} \kappa_x \\ \kappa_y \end{matrix} \right| & \text{for } -\frac{1}{2}N_x \leq \kappa_x \leq \frac{1}{2}N_x, \\ & \text{for } -\frac{1}{2}N_y \leq \kappa_y \leq \frac{1}{2}N_y, \end{cases} \quad (4)$$

where N_i is the number of grid points in each spatial direction [17], and $u_{x,y}$ is used to denote separate treatment of the longitudinal and transverse velocity components. We select a circular filter in wavenumber space with radius equal to the wavenumber limit that is resolved by the first-pass SR. Herein, we choose (empirically) $k = 35$.

Figure 2 shows a given sample of turbulent flow passed through a low-pass filter and high-pass filter at $k = 35$ in wavenumber space. These samples are then transformed back to physical space using a 2D inverse FFT (Figure 3). We include additional filtering to highlight the relative orders of magnitude between wavenumber ranges. We hypothesise that this may contribute to difficulties encountered in capturing higher-frequency components in super-resolved turbulence [1, 3, 18]; p-norm based loss functions in ML approach converge on orders of magnitude significantly lower than the amplitude of these wavenumbers in physical space, which makes recovery of information beyond this difficult.

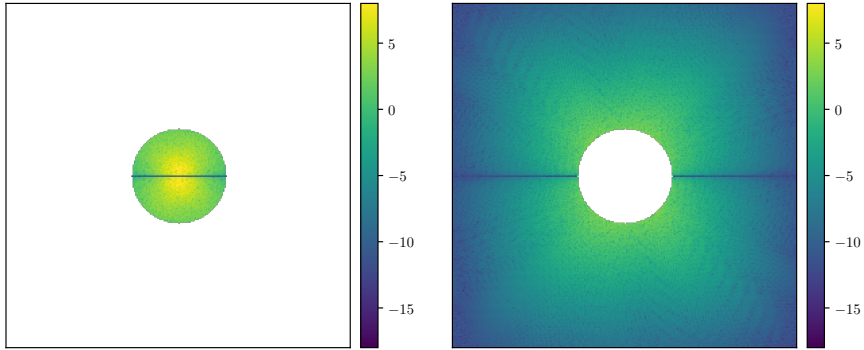


Figure 2: Spectral filters applied to a given 2D sample of the Kolmogorov flow, at $k \leq 35$ and $k > 35$. The field shown here is $\log(|\text{FFT}_{x,y}(u_x)|)$, which is the log magnitude of the 2D FFT amplitude.

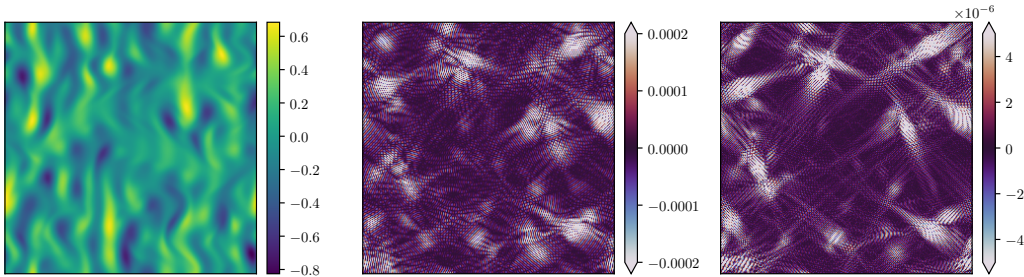


Figure 3: u_x , passed through spectral filters: $k \leq 64$ (left), $k > 64$ (center), $k > 96$ (right). We note the changing magnitude of each field, illustrating the numerical difficulty in capturing these components. Colour bars for the High-Pass Filtered (HPF) samples are scaled to better illustrate dominant fluctuations.

Fourier-filtering provides a new dataset used for training the stage two model, i.e., the spectral filtered diffusion model. During training, the model is shown the velocity fields passed through a Low-Pass Filter (LPF), and High-Pass Filter (HPF), and trained to predict noise content in high-frequency fields conditioned on low-frequency information. In a similar approach to that outlined above, given pure Gaussian noise and a low-frequency field obtained by filtering the first stage super-resolution, the model is then able to generate new samples of high-frequency complement information conditional on the generated low-frequency fields.

The full dataset preparation, training, and inference process is detailed in Figure 4.

3 Results

3.1 Spatial Super-Resolution of a Kolmogorov Flow

Here we present the results of a spatial super-resolution diffusion model trained to learn the distribution of high-resolution fields, u_i , given low-resolution representations of the fields. We train a DDPM (specifically SR3 [10]) to reconstruct a 256×256 field from a 32×32 low-resolution sample obtained by average-pooling the DNS solution. We examine a variety of quantitative and qualitative metrics to determine the extent to which turbulence has been recovered in our approach, on a validation dataset.

The vorticity, $\omega = \nabla \times \mathbf{u}$, is computed using an 8th order finite differencing in physical space for the high-resolution and a 2nd order approximation for the low-resolution. We should anticipate an approximately symmetric distribution of vorticity centred at 0 for individual samples.

From Figure 5, we observe that after the first stage of super-resolution, on an $8 \times$ upsampling task from 32×32 to 256×256 points, the flow structures are recovered well. The characteristic interactions

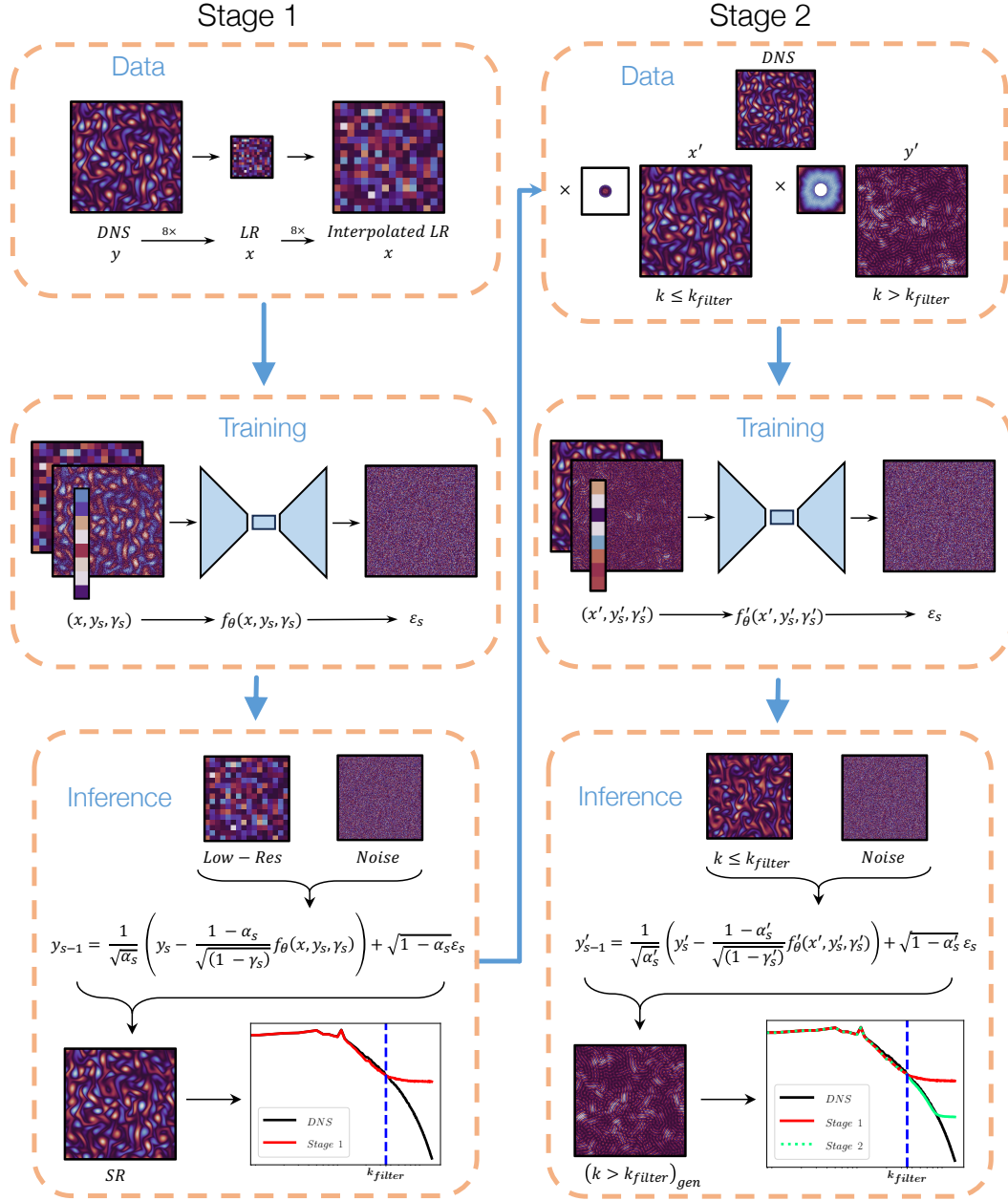


Figure 4: Procedure for spectrally decomposed turbulence generation. In stage 1, DNS data is downsampled to produce pairs of low and high resolution samples (x, y) . A DDPM, f_θ is trained to predict Gaussian noise in noisy high-resolution samples, y_s , conditioned on the low-resolution sample x , and the noise level γ_s . The trained DDPM is then used in inference to upsample new snapshots of turbulent flow. TKE spectra of the generated samples are compared against those of the DNS, giving a ‘cutoff’ wavenumber, k_{filter} . In stage 2, k_{filter} is used to filter the DNS in wavenumber space to obtain pairs of low and high pass filtered velocity fields, (x', y') . These are then used to train a second DDPM, f'_θ . This may then be used in inference to obtain a generated high-pass filtered field, conditional on the low-pass filtered field from stage 1 generation. TKE spectra indicate that stage 2 allows for accurate generation of higher-wavenumber turbulent structures than the stage 1 method allows for alone.

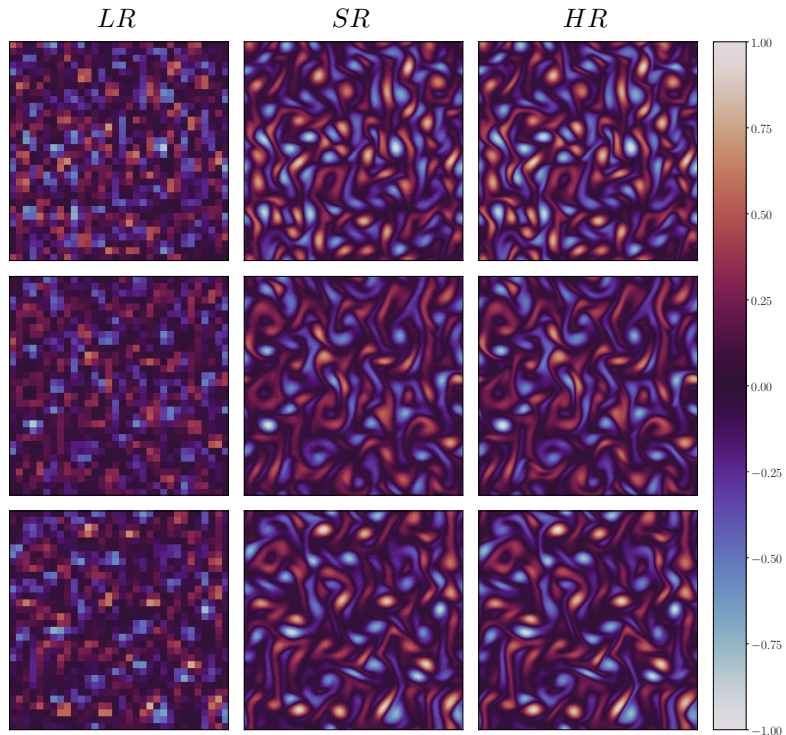


Figure 5: Contours of $\omega^* = \frac{\omega}{\omega_{max}}$ for the first stage spatial super-resolution, for three representative samples. The 32×32 [left] is super-resolved using a diffusion model to 256×256 [middle], which we compare to the ground truth DNS field [right].

between positive and negative vortices are also captured well, with clockwise and counterclockwise rotating structures. We note that the aim in generative super-resolution is not to produce a like-for-like version of the high-resolution sample, but to learn an underlying statistical description of the high-resolution data. To this end, some perceptual difference is acceptable, provided the generated and ground truth samples are statistically similar. Visible in the figure is the presence of some slight noise, which is likely to be a byproduct of the diffusion process. Our preliminary findings indicate that this can be mitigated through more extensive hyperparameter tuning.

The treatment of flow variables as continuous random variables implies that they are completely characterised by their PDF – rather than deterministically attempting to predict the value at a timestep, it is more sensible to consider the likelihood of a variable taking a certain value. We show the PDF of vorticity in Figure 6, presented on a log scale to better highlight values at the extreme ends of the scale. We observe that the super-resolved data shows good agreement with the high resolution data. This demonstrates the super-resolved fields are statistically similar to the ground truth DNS.

In order to investigate the recovery of information at all length scales of turbulence, we must examine the turbulent kinetic energy spectra. Figure 7 shows that through a learnt $8\times$ upsampling, the spatial SR diffusion model is able to recover wavenumbers in the range $16 < k \leq 35$, after which the SR solution diverges, as we would expect from the literature. Results from [9] indicate diffusion-based recovery to higher wavenumbers than this, but we could not reproduce their work on our fully decorrelated dataset; the authors omitted a detailed discussion on the level of correlation between

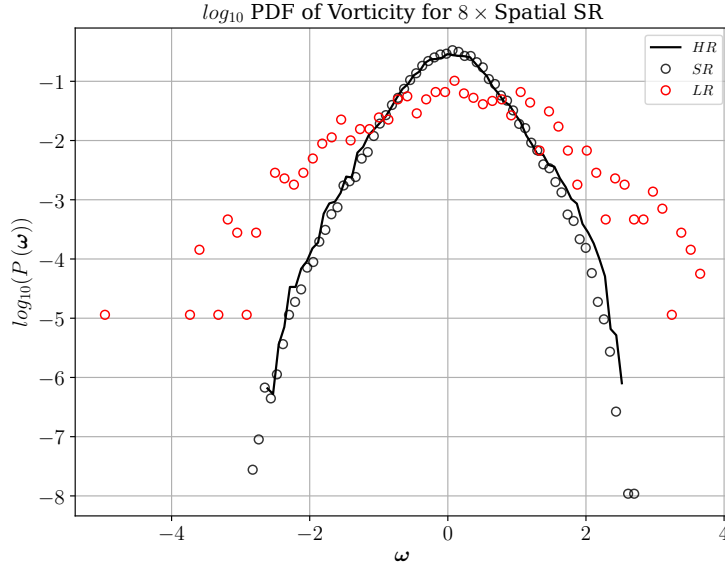


Figure 6: $\log_{10}(P(\omega))$ for the first stage spatial super-resolution, for a representative sample. LR is 32×32 , HR is the 256×256 DNS, and SR is from the super-resolved fields.

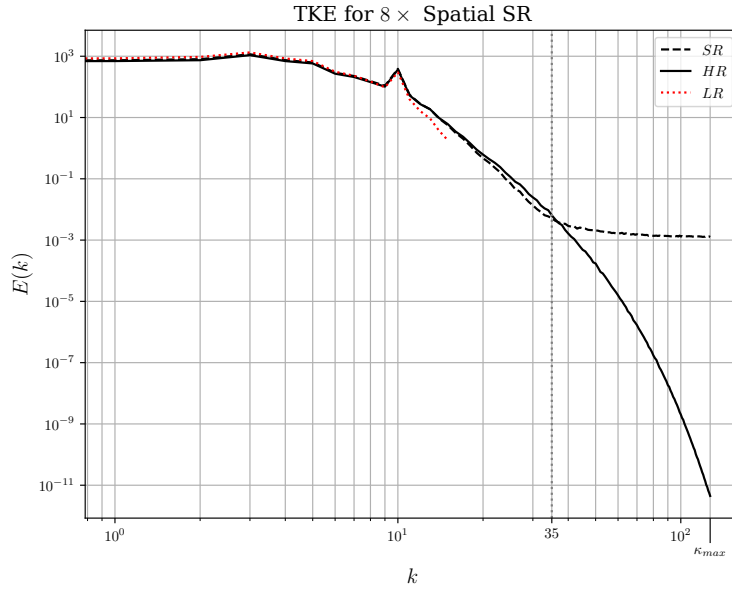


Figure 7: TKE Spectra from the single-stage super-resolution. LR is 32×32 , HR is the 256×256 DNS, and SR is from the super-resolved fields.

their training and validation sets. The recovered wavenumber limit is shown with a grey dashed line. The missing information beyond $k = 35$ may be explained by the numerical limitations in learning information at the high wavenumbers (§2.3), and limited model capacity (due to training limitations).

3.2 Fourier-Filtered Turbulence Generation

It is evident that the high wavenumber turbulent structures are difficult to capture due to their small contribution to the flow structure, notwithstanding their significant contribution to the flow statistics.

Both perceptually and from the probability distribution, it seems that turbulence recovery up to $k = 35$ appears to be sufficient for reasonable first order statistics. However, spectral analysis has shown that there is still non-negligible energy within these high wavenumbers, and for the purposes of scale-resolving simulations, these wavenumbers are considered significant. Here we demonstrate that using information from the spectrum of the spatially super-resolved flow, a second stage of turbulence recovery can be executed using a diffusion model trained to generate high-wavenumber flow components conditioned on their low-wavenumber complement.

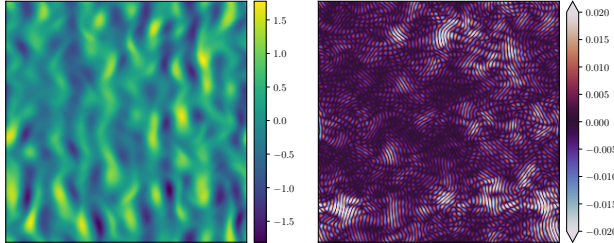


Figure 8: Representative sample of u_x with $k \leq 35$ (left), and $k > 35$ (right), prior to standardisation.

From Figure 7, we identify the line at $k = 35$ as the wavenumber at which the super-resolved field starts to diverge from the reference DNS solution. The recovery up to this wavenumber is strong. As such, we take a spectral filter (Figure 2) and apply it to the 2D FFT of the velocity field, i.e., the velocity field in wavenumber space. We then convert the fields back to physical space, obtaining low-wavenumber, high-wavenumber pairs as in Figure 8. The conversion back to physical space is required as the generative model is not guaranteed to produce real (i.e. non-complex) fields if generating in wavenumber space. A key feature of this form of filtering operation is that the sum of the low-wavenumber and high-wavenumber field in physical space is equal to the ground truth DNS field; this is exploited in order to use this approach for high-wavenumber correction of the spatial super-resolution.

The high-wavenumber flow fields are presented in Figure 9. The generated high-wavenumber fields show strong agreement with the ground truth DNS high-wavenumber fields. This lends credence to the conjecture that high-wavenumber recovery using diffusion models is made possible by isolating and rescaling high-wavenumber information. As before, we analyse spectral information to ascertain the turbulence recovery in wavenumber regions of interest, as in Figure 10.

The red dashed line indicated on figure 10 shows the TKE spectrum for the high-wavenumber component of the DNS flow. We demonstrate that our spectral decomposition diffusion model is able to recover turbulence information in this region up to $k = 74$, which means that through the first and second stage of turbulence generation, our method recovers a reasonable portion of the wavenumbers simulated in the DNS. We anticipate that a general N-stage model would iteratively be able to recover the whole spectrum, but leave this exercise as future work. The number of stages, N, may be considered a hyperparameter which in this study we fix to 2.

4 Conclusions, Considerations, and Future Work

We have demonstrated that a diffusion model may be used as a generative technique to recover high-fidelity information lost from a high resolution field. We extend approaches to do so by using spectral filters in wavenumber space to decompose flow fields into high and low wavenumber components, training a diffusion model to learn the conditional probability of a high-frequency field given a low-frequency field. We investigate the performance of our method by considering physical quantities recovered in the super-resolved flow. We find that diffusion models are a powerful generative method for super-resolution of turbulence, and that strong statistical recovery of turbulence can be achieved by the developed method.

We have omitted a discussion on inference cost in diffusion models, but a key open issue in this area is the fact that as compared to other generative methods which require (typically) a single network evaluation through their parameterising network, the iterative nature of diffusion models necessitates multiple network evaluations. Denoising Diffusion Implicit Models (DDIM) aim to

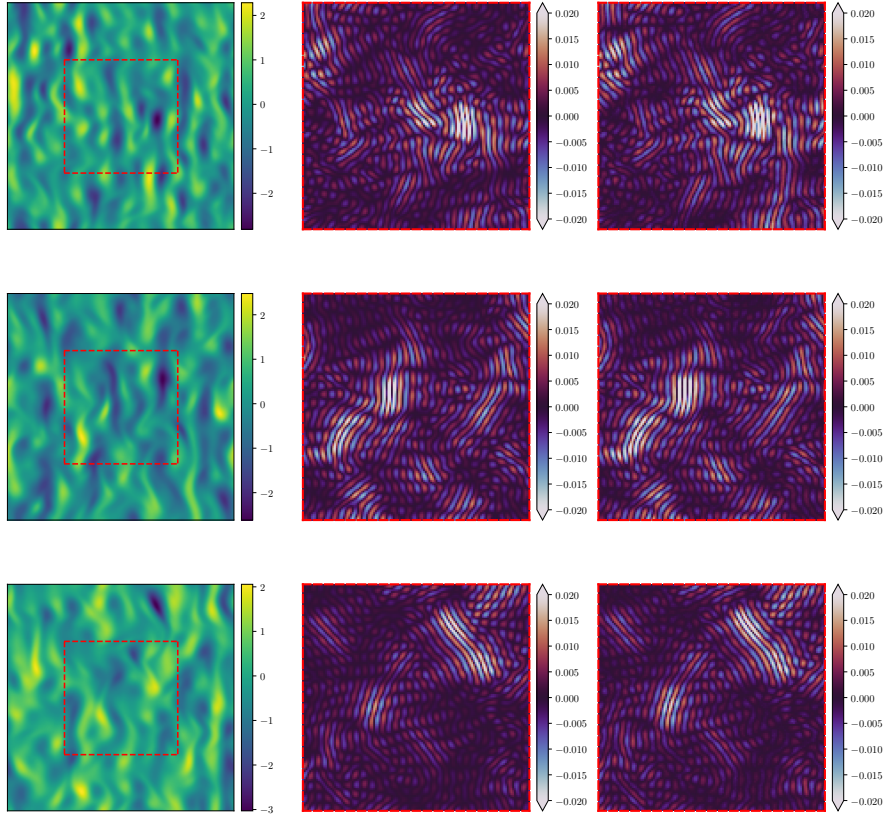


Figure 9: $u_x(k \leq 35)_{GEN}$ [left], $u_x(k > 35)_{DNS}$ [middle], $u_x(k > 35)_{GEN}$ [right] at three representative timesteps. *GEN* is used for generated fields from the first and second stage diffusion models. Middle and right columns show fields that are centre-cropped for clarity – largest values occur nearer the boundaries and obscure main-field oscillations. The crop location is indicated on the low-wavenumber fields in the left column by the red dashed line, which corresponds to the boundary in the middle and right column.

address this by driving down the number of network evaluations through a novel sampling approach [19]. Additionally, we note that our two-stage turbulence recovery approach is equally applicable to other generative methods, such as GANs.

Additionally, there has been substantial work on exploring the impact of noising schedules. We ran a simple grid search over the reverse schedule to determine the ideal reverse variance schedule for generation, but due to resource constraints we did not consider multiple forward schedules. There is evidence to suggest that the noising schedule has a significant impact on the generative capabilities of a diffusion model, and warrants further examination [13].

A limitation of this approach to filtering in wavenumber space for a second stage of turbulence recovery is that the filter is dependent on the wavenumbers recovered in the first stage super-resolution. This has a direct impact on training time; the first and second stage diffusion models cannot be trained in parallel and must be trained sequentially after testing the performance of the first stage spatial super-resolution model. We propose that our method may be extended by using a reverse process designed to recover specific wavenumbers, which may be known *a priori* and thus allowing for the second stage high-wavenumber diffusion model to be trained in parallel. This would also enable the use of variable wavenumber cutoffs for regions where the flow is resolved well vs regions where it is less well resolved.

We propose that this method could be extended to investigate specified ranges of wavenumber space. Spherical shells or doughnut shaped filters in 3D and 2D respectively allow for the decomposition of a flow into its constituent wavenumber modes. We believe that recursively applying corrections at

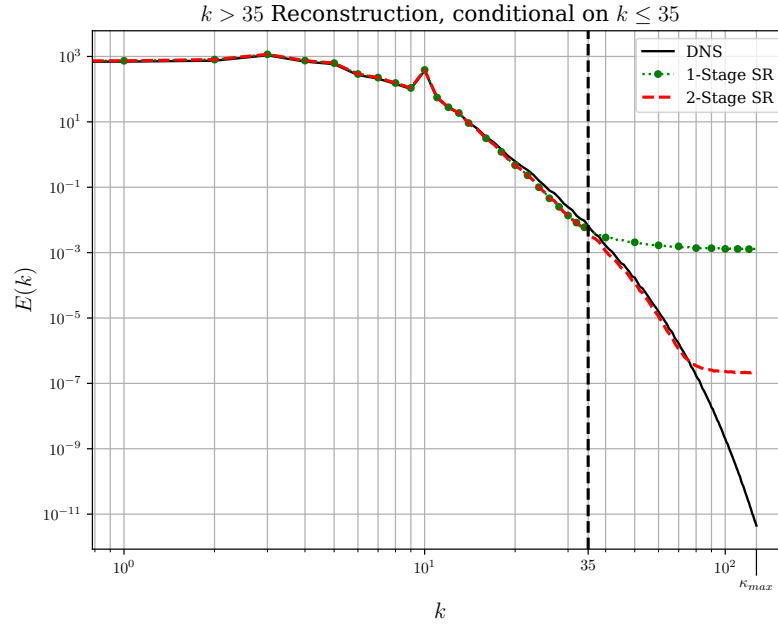


Figure 10: TKE spectra from high-wavenumber conditional turbulence generation. The sum of low and high wavenumber components of the reconstructed flow is compared to the DNS field.

different wavenumber ranges may be a viable option for subgrid-scale modelling using lower-fidelity CFD methods, where the maximum simulated wavenumber is less than the maximum wavenumber for a DNS-like solution.

5 Acknowledgements

The authors would like to acknowledge the assistance given by Research IT and the use of the Computational Shared Facility at The University of Manchester. The authors would also like to personally thank Daniel Kelshaw at Imperial College London for fruitful conversations regarding spectral decomposition. SD acknowledges a Dame Kathleen Ollerenshaw Fellowship.

References

- [1] Kai Fukami, Koji Fukagata, and Kunihiko Taira. Super-resolution reconstruction of turbulent flows with machine learning. *Journal of Fluid Mechanics*, 870:106–120, July 2019. ISSN 0022-1120, 1469-7645. doi: 10.1017/jfm.2019.238.
- [2] Bo Liu, Jiupeng Tang, Haibo Huang, and Xi-Yun Lu. Deep learning methods for super-resolution reconstruction of turbulent flows. *Physics of Fluids*, 32(2):025105, February 2020. ISSN 1070-6631. doi: 10.1063/1.5140772.
- [3] Hyojin Kim, Junhyuk Kim, Sungjin Won, and Changhoon Lee. Unsupervised deep learning for super-resolution reconstruction of turbulence. *Journal of Fluid Mechanics*, 910:A29, March 2021. ISSN 0022-1120, 1469-7645. doi: 10.1017/jfm.2020.1028.
- [4] Claudia Drygala, Benjamin Winhart, Francesca di Mare, and Hanno Gottschalk. Generative Modeling of Turbulence. *Physics of Fluids*, 34(3):035114, March 2022. ISSN 1070-6631, 1089-7666. doi: 10.1063/5.0082562.
- [5] B. Galanti and A. Tsinober. Is turbulence ergodic? *Physics Letters A*, 330(3-4):173–180, September 2004. ISSN 03759601. doi: 10.1016/j.physleta.2004.07.009.

- [6] Jonathan Ho, Ajay Jain, and Pieter Abbeel. Denoising Diffusion Probabilistic Models, December 2020.
- [7] Zhisheng Xiao, Karsten Kreis, and Arash Vahdat. Tackling the Generative Learning Trilemma with Denoising Diffusion GANs, April 2022.
- [8] Prafulla Dhariwal and Alex Nichol. Diffusion Models Beat GANs on Image Synthesis, June 2021.
- [9] Dule Shu, Zijie Li, and Amir Barati Farimani. A physics-informed diffusion model for high-fidelity flow field reconstruction. *Journal of Computational Physics*, 478:111972, April 2023. ISSN 00219991. doi: 10.1016/j.jcp.2023.111972.
- [10] Chitwan Saharia, Jonathan Ho, William Chan, Tim Salimans, David J. Fleet, and Mohammad Norouzi. Image Super-Resolution via Iterative Refinement, June 2021.
- [11] N. Platt, L. Sirovich, and N. Fitzmaurice. An investigation of chaotic Kolmogorov flows. *Physics of Fluids A: Fluid Dynamics*, 3(4):681–696, April 1991. ISSN 0899-8213. doi: 10.1063/1.858074. URL <https://pubs.aip.org/pof/article/3/4/681/402184/An-investigation-of-chaotic-Kolmogorov-flows>.
- [12] Gideon Dresdner, Dmitrii Kochkov, Peter Norgaard, Leonardo Zepeda-Núñez, Jamie A. Smith, Michael P. Brenner, and Stephan Hoyer. Learning to correct spectral methods for simulating turbulent flows. 2022. doi: 10.48550/ARXIV.2207.00556. URL <https://arxiv.org/abs/2207.00556>.
- [13] Ting Chen. On the Importance of Noise Scheduling for Diffusion Models, May 2023.
- [14] Olaf Ronneberger, Philipp Fischer, and Thomas Brox. U-Net: Convolutional Networks for Biomedical Image Segmentation, May 2015.
- [15] Giannis Daras, Yuval Dagan, Alexandros G. Dimakis, and Constantinos Daskalakis. Consistent Diffusion Models: Mitigating Sampling Drift by Learning to be Consistent, February 2023. URL <http://arxiv.org/abs/2302.09057>. arXiv:2302.09057 [cs, math].
- [16] Chieh-Hsin Lai, Yuhta Takida, Naoki Murata, Toshimitsu Uesaka, Yuki Mitsufuji, and Stefano Ermon. FP-Diffusion: Improving Score-based Diffusion Models by Enforcing the Underlying Score Fokker-Planck Equation, June 2023. URL <http://arxiv.org/abs/2210.04296>. arXiv:2210.04296 [cs].
- [17] Stephen B. Pope. *Turbulent Flows*. Cambridge University Press, 2000. doi: 10.1017/CBO9780511840531.
- [18] Daniel Kelshaw, Georgios Rigas, and Luca Magri. Physics-Informed CNNs for Super-Resolution of Sparse Observations on Dynamical Systems, November 2022.
- [19] Jiaming Song, Chenlin Meng, and Stefano Ermon. Denoising Diffusion Implicit Models, October 2022.